Analysis of multicomponent LFM signals by Teager-Huang-Hough Transform

Abdelkhalek Bouchikhi, Abdelouahab Boudraa, Jean-Christophe Cexus, Thierry Chonavel

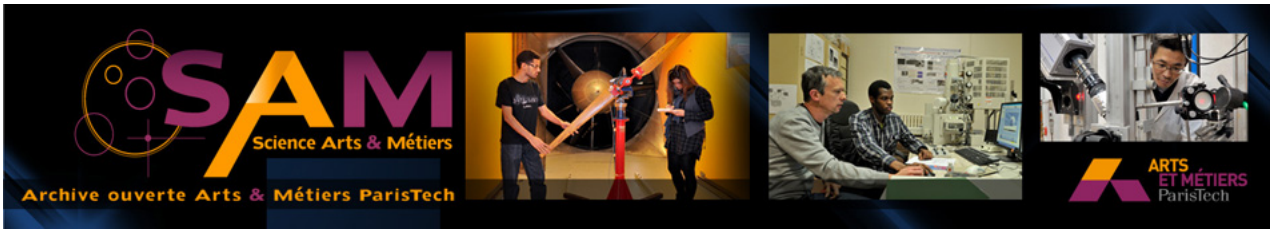

Analysis of Multicomponent LFM Signals by Teager Huang-Hough Transform

ABDELKHALEK BOUCHIKHI
ABDEL-OUAHAB BOUDRAA, Senior Member, IEEE
Ecole Navale
France

JEAN-CHRISTOPHE CEXUS
ENSTA Bretagne
France

THIERRY CHONAVEL, Member, IEEE
Télécom Bretagne
France

A novel detection approach of linear FM (LFM) signals, with single or multiple components, in the time-frequency plane of Teager-Huang (TH) transform is presented. The detection scheme that combines TH transform and Hough transform is referred to as Teager-Huang-Hough (THH) transform. The input signal is mapped into the time-frequency plane by using TH transform followed by the application of Hough transform to recognize time-frequency components. LFM components are detected and their parameters are estimated from peaks and their locations in the Hough space. Advantages of THH transform over Hough transform of Wigner-Ville distribution (WVD) are: 1) cross-terms free detection and estimation, and 2) good time and frequency resolutions. No assumptions are made about the number of components of the LFM signals and their models. THH transform is illustrated on multicomponent LFM signals in free and noisy environments and the results compared with WVD-Hough and pseudo-WVD-Hough transforms.

Manuscript received April 8, 2012; revised December 20, 2012; released for publication July 9, 2013.

DOI. No. 10.1109/TAES.2014.120202.

Authors' addresses: A. Bouchikhi, A. O. Boudraa, Ecole Navale, BCRM Brest, CC 600, 29240 Brest Cedex 9, France. E-mail: (abouchik@hotmail.fr). J. C. Cexus, ENSTA Bretagne, 2 rue François Verny, 29806 Brest Cedex, France; T. Chonavel, Institut Télécom, Télécom Bretagne, Technopole Brest-Iroise, 29238 Brest Cedex 3, France.

I. INTRODUCTION

Linear frequency modulated (LFM) signals, also known as chirp signals, are frequently encountered in many applications such as radar, sonar, and telecommunications. For example, due to target motion, radar return signals can be modeled as LFM signals, the parameters of which reveal useful information about the target such as velocity and acceleration [1]. Detection and estimation of the parameters of such signals are very important for electronic intelligence applications [2–4]. Although the generalized likelihood ratio test has been reported to be optimal for chirp detection [5], it requires too much computational complexity to support practical applications [6]. Methods based on the maximum likelihood (ML) estimator [7, 8] are also used, but heavy computational complexity is generally needed for high estimation accuracy [9]. Time-frequency-based methods have been reported to be effective for detecting and estimating LFM signals [10, 11]. These techniques have attracted considerable attention and proved themselves to be effective among others [12]. The first time-frequency approach involved spectrogram [11]. However, the spectrogram suffers from fixed time and frequency resolutions due to the fixed window length and is not a totally cross-terms free representation [13] which limits its application to LFM detection. Wavelet transforms can also be used for LFM detection because they are not limited by the fixed window constraint. However, it suffers from poor frequency resolution [13]. Due to its high time-frequency localization, Wigner-Ville distribution (WVD) is optimal in the sense of maximum energy concentration about the instantaneous frequency (IF), for LFM signals [13]. For such signals, the detection approach computes the line integral of the WVD along all the lines in the time-frequency plane. The line that produces the maximum value yields to the ML estimate of the linear IF of the chirp. Thus, the principle of the method is to track straight lines in the time-frequency plane by locating maxima in the two-dimensional (initial frequency versus chirp rate) plane [12]. This detection can be obtained by combining the WVD with Hough transform [10] or Radon transform [12–14]. Due to its bilinear nature, WVD involves cross-product terms, which appear midway between true signal components (auto-terms) in the case of multicomponent signals. These cross-terms make the transform space of VWD difficult to visually interpret.

Recently, a new time-frequency representation for analyzing multicomponent AM-FM signals referred to as Teager-Huang (TH) transform has been introduced [15]. Compared with WVD, TH transform shows further benefits: fine time-frequency resolution and free of cross-terms. TH transform relies on no prior choice upon the number of AM-FM components of the analyzed signal. Further, it is based on adaptive basis and is not constrained by uncertainty principle. In this work, we present a novel detection approach of multicomponent LFM signals, based on a time-frequency domain representation of TH

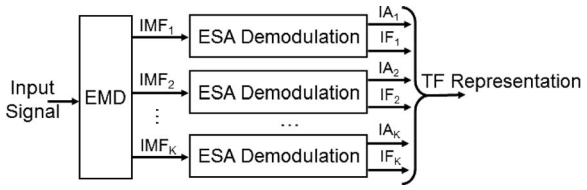

Fig. 1. Block diagram of TH transform.

transform, that we named Teager-Huang-Hough (THH) transform.[1] Compared with our previous work [16] where THH transform was limited to noise-free signals, the present work contributions are the following.

1) THH transform is analyzed in noisy conditions. For this analysis, subband filtering associated to THH transform is introduced in Section VI.
2) Teager-Kaiser spectrum is introduced in Subsection II-C.
3) A mathematical formulation of THH transform is introduced (11).
4) A strategy for deriving the detection threshold is presented in Subsection IV-B.

II. TEAGER-HUANG TRANSFORM

TH transform has been introduced recently for time-frequency analysis [15]. It has found applications in a lot of domains [17–22]. This transform first band-pass filters a multicomponent AM-FM signal through the empirical mode decomposition (EMD) into a reduced number of oscillatory modes called intrinsic mode functions (IMFs) [23]. Each extracted mode is demodulated into IF and instantaneous amplitude (IA) signals. An energy demodulation method, called energy separation algorithm (ESA) [23], is used to simultaneously track these IF and IA components. The ESA is based on Teager-Kaiser energy operator (TKEO) and shows high efficiency, in particular in terms of time resolution. More particularly, TKEO is attractive due to its computational simplicity and because it tracks physically meaningful quantities. Applying ESA to IMFs yields IFs as a function of time that enables sharp identifications of embedded structures of the signal. Taken collectively, the spectra of the IMFs supplied by ESA yield complete time-frequency information (energy) about the original signal. A common method for displaying the spectra derived from the IMFs, is to generate a two-dimensional plot with time and frequency axes. The block diagram of TH transform, depicting multiband filtering followed by energy separation is shown in Fig. 1.

A. EMD

The EMD has been introduced by Huang et al. [23] for adaptively decomposing any signal into a reduced number of IMFs and a residual that represents the trend. By definition, an IMF 1) must have the same numbers of extrema and zero-crossing or differ at most by one; and 2) is symmetric with respect to local zero mean. With these two conditions, meaningfully IF and IA components of an IMF can be well defined. In order to successfully decompose a signal $x(t)$ into IMFs, it must have at least two extrema (one maximum and one minimum). Given conditions 1 and 2, EMD is defined by an iterative process called sifting and is summarized as follows [23].

1) Identify the extrema of signal $x(t)$.
2) Generate its upper and lower envelopes, $x_u(t)$ and $x_l(t)$, with spline interpolation.
3) Compute the local mean $m(t) = (x_u(t) + x_l(t))/2$.
4) Extract the detail $d(t) = x(t) – m(t)$.
5) Check the properties of $d(t)$.

If $d(t)$ meets conditions 1 - 2, an IMF is derived and $r(t) \leftarrow x(t) – d(t)$.
If $d(t)$ is not an IMF, $x(t) \leftarrow d(t)$.

6) Repeat steps 1 - 5 until $r(t)$ satisfies some stopping criterion.

At the end of the process, $x(t)$ is expanded as follows:

$$x(t) = \sum_{j=1}^{K} \mathrm{IMF}_j(t) + r_K(t) \tag{1}$$

where K is the number of IMFs and $r_K(t)$ denotes the final residue. The IMFs are nearly orthogonal to each other, and all have nearly zero means. The number of extrema is decreased when going from one mode to the next, and the whole decomposition is guaranteed to be finished with a finite number of modes.

B. Energy Separation of IMFs

The salient property of an IMF is that it is a monocomponent AM-FM signal [23] and therefore it can be demodulated using ESA. For a twice derivable signal $s(t)$, the output of TKEO is given by

$$\Psi[s(t)] = [\dot{s}(t)]^2 - s(t)\ddot{s}(t) \tag{2}$$

where $\dot{s}(t)$ and $\ddot{s}(t)$ are the first and second order derivatives of $s(t)$. A useful and important property of $\Psi[.]$ is its behavior when applied to AM-FM signal $s(t)$ in the form

$$s(t) = a(t)\cos\left(2\pi \int_0^t f(\tau)d\tau\right). \tag{3}$$

Then, the output of $\Psi[.]$ applied to $s(t)$ and $\dot{s}(t)$ is given by

$$\Psi\,[s(t)] \approx a^2(t)\dot{\phi}^2(t) \tag{4}$$

$$\Psi\,[\dot{s}(t)] \approx a^2(t)\dot{\phi}^4(t). \tag{5}$$

Thus, with negligible approximation error under general realistic conditions, (4) shows that $\Psi[s(t)]$ is the squared product of $a(t)$ and the time-varying instantaneous phase

[1]Some elements of this paper were initially presented in [16].

$\dot{\phi}(t)$. Combining relations (4) and (5) we obtain the ESA method [24]:

$$f(t) \approx \frac{1}{2\pi}\sqrt{\frac{\Psi\,[\dot{\mathrm{s}}(t)]}{\Psi\,[\mathrm{s}(t)]}},\ |a(t)| \approx \frac{\Psi\,[\mathrm{s}(t)]}{\sqrt{\Psi\,[\dot{\mathrm{s}}(t)]}}. \quad (6)$$

A discrete-time counterpart of the TKEO $\Psi_d[.]$ is given by [24]

$$\Psi_d[\mathrm{s}(n)] = \mathrm{s}^2(n) - \mathrm{s}(n+1)\cdot\mathrm{s}(n-1). \quad (7)$$

Equation (7) shows that TKEO is nearly instantaneous because only three samples are required for the energy computation at each time instant. By approximating the continuous-time derivation in (4)–(5) to discrete differences, one obtains different versions of discrete ESA (DESA) [24]. For example, by approximating the continuous-time derivatives in (6) by discrete asymmetric backward differences, one obtains the DESA-1a algorithm:

$$f(n) \approx \frac{1}{2\pi}\arccos\left(1 - \frac{\Psi_d[\mathrm{s}(n) - \mathrm{s}(n-1)]}{2\Psi_d[\mathrm{s}(n)]}\right) \quad (8)$$

$$|a(n)| \approx \sqrt{\frac{\Psi_d[\mathrm{s}(n)]}{1 - \left(1 - \frac{\Psi_d[\mathrm{s}(n) - \mathrm{s}(n-1)]}{2\Psi_d[\mathrm{s}(n)]}\right)^2}}. \quad (9)$$

Other DESAs can be derived [24].

C. Teager-Kaiser Spectrum

After applying DESA to each IMF component of a signal $\mathrm{x}(t)$, one can express it in the following form:

$$\mathrm{x}(t) = \Re\left(\sum_{j=1}^{K} a_j(t)\exp\left(i\int \omega_j(t)dt\right)\right) + r_K(t) \quad (10)$$

where $\Re$ stands for "real part", $\omega_j(t) = 2\pi f_j(t)$ and $i = \sqrt{-1}$. If we omit $r_{\mathrm{K}}(t)$, which is either a monotonic function or a constant, representation (10) gives both amplitude and frequency of each component as functions of time. This equation enables us to represent IA and IF as functions of time in a three-dimensional plot: for each IMF, we get a curve $(t, f_i(t), a_i(t))$. The weight assigned to each time-frequency cell is the local spectrum amplitude. We call the amplitude (or energy) depending on time and frequency the Teager-Kaiser spectrum (TKS), $\mathrm{TK}(t, f)$. Formally, this is defined as follows. Let signal $\mathrm{x}(t)$ be represented in the form (10). The TKS (amplitude) is defined as

$$\mathrm{TK}(t, f) := \begin{cases} a_1(t) & \text{on the curve } \{(t,\ f_1(t));\ t \in \mathbb{R}\} \\ a_2(t) & \text{on the curve } \{(t,\ f_2(t));\ t \in \mathbb{R}\} \\ \vdots & \\ a_K(t) & \text{on the curve } \{(t,\ f_K(t));\ t \in \mathbb{R}\} \end{cases}$$

Given IFs, $f_j(t)$, and IAs, $a_j(t)$, at each instant t, associated time-frequency of TH transform can be written as

$$\mathrm{TK}(t, f) = \sum_{j=1}^{K} aj(t, fj(t)) = \sum_{j=1}^{K} aj(t)\delta(f - f_j(t)). \quad (11)$$

An advantage of TKS analysis over Hilbert spectral analysis [23] is to circumvent the limitation of Bedrosian's theorem [25]. TH transform produces a sharp and sparse representation. If $x(t)$ is of dimension T in time and is given in discrete-time, its time-frequency representation is of dimension N_fT when computed over N_f frequency bins. Since the number of extracted modes (Eq. 1), K, is much smaller than T, TH transform which satisfies relation (11) is distributed over the time-frequency plane in a very sparse way, with only K 1D trajectories where at most KT values are expected to be non-zero. All information of the TH transform is concentrated in a very small number of 1D trajectories. Thus, in terms of number of points, TH transform is of KT dimensions where $K \ll T$ while, for example, WVD is of dimension TN_f.

III. HOUGH TRANSFORM

Hough transform is a feature extraction technique essentially used in image processing for detecting geometric curves (lines, circles ...) in binary point images such as object detection [26] and texture analysis. Note that since the Cartesian representation $y = ax + b$ of a line becomes clumsy [26] as a line approaches the vertical, alternative polar representation can be preferred [26]. The key idea of Hough transform is to project pixels of a given image into a parametric space where the shapes of interest can be well localized. For example, for line detection and polar parametrization we have

$$HT(x_i, y_i) = \{(\rho, \theta);\ \rho = x_i\cos\theta + y_i\sin\theta\}. \quad (12)$$

This parametrization specifies a straight line by the angle θ of its normal and its algebraic distance ρ from the origin. For each point (x_i, y_i) in an image, Hough transform associates a sinusoid in the plane (ρ, θ), with amplitude $\sqrt{x_i^2 + y_i^2}$ and initial phase $\arctan(y_i/x_i)$. In addition, the pixels of the sinusoid are given an intensity equal to that of the pixel (x_i, y_i). If M points are concentrated along a straight line in time-frequency domain, their transforms will define M sinusoidal curves that intersect at the same point in the (ρ, θ) domain (Fig. 2) where curve intensities add. Thus, maxima location in the Hough transform domain are directly related to the parameters of the lines in the initial image and the Hough transform converts a difficult global detection problem in image domain into a more easily solved local peak detection problem in the parameters space.

IV. TH AND HOUGH TRANSFORMS

A. Hough Transform for LFM Signals

Different methods have been proposed for LFM component tracking using time-frequency representations

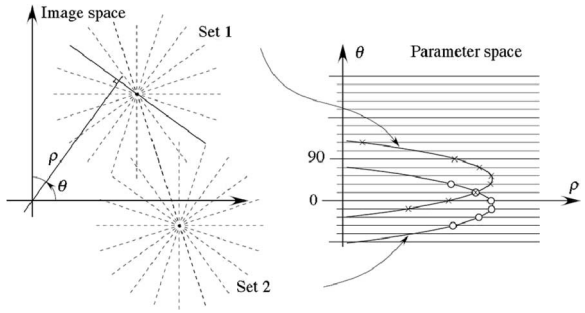

Fig. 2. Illustration of Hough transform.

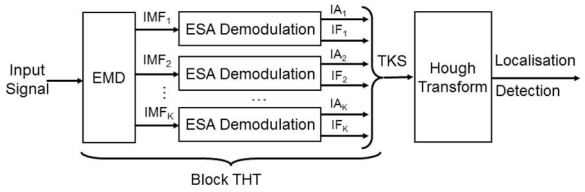

Fig. 3. Block diagram of THH transform.

[9–12, 14, 27–30]. A time-frequency representation is viewed as an image, where a pixel intensity corresponds to the energy presents at a particular time and frequency positions. The combination of WVD and Hough transform was first presented for chirp identification [10]. WVD ideally concentrates the chirp signals in time-frequency plane. FM parameters can be estimated using Hough transform combined with WVD [10], smoothed pseudo-WVD (SPWVD) [27], or reallocated SPWVD (RSPWVD) [28]. The principle of the method has been introduced by Kay and Boudreaux-Bartles [29], extended to the multicomponent case by Barbarossa [10], and also extended to analysis of constant amplitude signals (cross-terms) added to a spread spectrum plus an additive white Gaussian noise (AWGN) by Barbarossa and Scaglione [30]. In general, the detection problem of an LFM signal, which is not easy in the time-domain (or frequency domain), is reduced to the detection of a line in an image. Applying a Hough transform in the time-frequency representation of a multiple components LFM signal yields peaks in the Hough space, the coordinates of which are directly related to the parameters of the straight lines in time-frequency image. Although the method is attractive, accurate estimation of FM parameters is not easy due to the cross-terms of the quadratic time-frequency representations (WVD, ...). This leads to difficulties in practical implementation, and the computational attractiveness of array accumulators of Hough transform was not advantageously utilized. Alternatively, the THH transform that we propose and that is illustrated in Fig. 3 is a time-frequency representation free of cross-terms and is used to detect energy-varying linear chirp. When Hough transform is applied to TH transform of an LFM signal $y(t)$ it outputs an energy time-frequency representation. Let $y(t)$ be such a signal:

$$\mathrm{y}(t) = e^{2i\pi\left(\nu t + \frac{\beta}{2}t^2\right)} \tag{13}$$

where ν is the start frequency of the LFM and β the chirp rate. The comparison of THH transform to a threshold τ enables LFM peaks detection. Estimates of the unknown parameters ν and β are given by the coordinates of the peak in the space of the parameters (ρ, θ).

THH transform of a signal $\mathrm{y}(t)$ is defined as the line integral through the TKS along the IF model $f(t; \Theta)$ where $\Theta := (\nu, \beta)$ is the parameter vector.

$$\mathrm{h}(\nu,\ \beta) = \int_{-\infty}^{-\infty} \mathrm{TK}(t,\ f)\delta(f - \nu - \beta t)dt \tag{14}$$

where $\mathrm{TK}(t, f)$ is the TKS under consideration. When dealing with LFM signals, each IMF gives rise to energy concentration along straight lines in the time-frequency plane of $f_j(t) \approx (t, \Theta_j) = \nu_j + \beta_j \mathrm{t}$, where $f_j(t)$ is the IF of the j^{th} IMF. The integration over all possible lines, obtained by applying Hough transform to TH transform gives rise to peaks in the final parameter space. A monocomponent LFM signal corresponds to one peak in the parameter space and a multicomponent LFM signal generates multiple peaks in the parameter space. THH transform is therefore a mapping from the time-frequency domain to the parameter space (ν, β). The detection and parameters estimation is reduced to peaks search in the parameter space. THH transform algorithm involves the following steps.

Step 1) Apply TH transform to input signal $\mathrm{x}(t)$ to generate $\mathrm{TK}(t, f)$ (11).
Step 2) Compute $\mathrm{h}(\Theta)$ using (14).
Step 3) Search peaks of $\mathrm{h}(\Theta)$ which are larger than τ.
Step 4) Extract parameters Θ of each detected peak.

Values of θ and ρ (12) are given by

$$\theta = \arctan(-1/\beta) \text{ and } \rho = \nu \sin(\theta).$$

Note that time-frequency localization of a signal can be quantified by the percentage of the time-frequency plane that it occupies. Since TH transform consists of a reduced number of 1D trajectories it is highly localized. Besides this sparsity, THH transform is based on two local and nonlinear approaches, the ESA (which in turn is based on the instantaneous TKEO) and the EMD. This enables THH transform to have a good time-frequency resolution and to perform good LFM localization and estimation.

B. Thresholding Based on Neyman-Pearson Criterion

Different criteria can be used to choose the detection threshold such as MiniMax, maximum a posteriori probability or Neyman-Pearson (NP) criterion. As NP rule does not involve decision costs or prior knowledge of LFM signals distribution, it is well suited for choosing a detection threshold τ. Then, the threshold is calculated for a targeted false alarm probability. The problem is to decide between the null hypothesis (H_0) and the

alternative one (H_1):

$$\begin{cases} H_1: & \text{a LFM component is present in TKS} \\ H_0: & \text{no LFM is present.} \end{cases}$$

Let τ denote the threshold for LFM component detection. For the K IMFs under consideration, $\text{IMF}_i(t)$ has IA $a_i(t)$ for $t = 1, \ldots, T$. For the sake of simplicity, let us assume an approximate circularly complex Gaussian distribution for the IMFs. Thus amplitudes $a_i(t)$ are Rayleigh distributed. In addition, to achieve simple in designing the threshold τ, it will appear more convenient to perform the Hough transform on the squared TKS where amplitude at point $(t, f_i(t))$ is $a_i^2(t)$ and has a $\chi^2(2)$ distribution, with mean $\mathbb{E}[a_i^2(t)]$ denoted by σ^2.

Let us now consider the all-at-one time-frequency representation, that is the area of the discretized time-frequency plane where the Hough transform is calculated, with all points set to one. Then, we denote by $N^0_{\nu\beta}$ the integer value of the Hough transform at point ($\nu = \rho/\sin(\theta)$, $\beta = -\cot(\theta)$) of the corresponding transformed plane. In other words, $N^0_{\nu\beta}$ represents the number of lines that pass through (ν, β) for the all-at-one time-frequency representation.

The support of the TKS is made of KT points, while the time-frequency representation contains $N_f T$ samples. Then, only a fraction

$$S = \frac{KT}{N_f T} = \frac{K}{N_f} \tag{15}$$

of the time frequency plane carries the TKS. Note that S represents the sparsity rate in the TKS. If there is no LFM (H_0 hypothesis) the Hough transform is unstructured and, on the average, there are $SN^0_{\nu\beta}$ lines passing through (ν, β). However, letting $N_{\nu\beta}$ be the number of lines at (ν, β), it is clear that its value can differ from $SN^0_{\nu\beta}$. A convenient modeling for $N_{\nu\beta}$ is to describe it as a Poisson random variable with mean $SN^0_{\nu\beta}$. Indeed, the number of lines passing through (ν, β) is a binomial distribution $\mathcal{B}(KT, p)$ where $p = \frac{N^0_{\nu\beta}}{N_f T}$ is the probability that the transform of a given point of the time-frequency plane generates a line passing through (ν, β). As KT is quite large, it is well known that $\mathcal{B}(KT, p)$ can be well approximated by a Poisson $\mathcal{P}(\lambda)$ distribution, with $\lambda = KTp = SN^0_{\nu\beta}$. Then, we get

$$P(N_{\nu\beta} = k) = \frac{\left(SN^0_{\nu\beta}\right)^k}{k!} e^{-SN^0_{\nu\beta}}. \tag{16}$$

For hypothesis H_0 and conditional to $N_{\nu\beta}$, the distribution of the amplitude $a_{\nu\beta}$ at point (ν, β) is that of the accumulation of $N_{\nu\beta}$ independent random amplitudes with distribution $\chi^2(2)$, that is, $a_{\nu\beta}$ has a $\chi^2(2N_{\nu\beta})$ distribution. Note that the normalized $\chi^2(n)$ distribution has variance $2n$ and the accumulation of $N_{\nu\beta}$ points $a_i(t)$ has variance $N_{\nu\beta}\sigma^2$. Thus a normalizing factor equal to $\sigma/2$ must be applied to the standard $\chi^2(2N_{\nu\beta})$ random variables to achieve the desired distribution. Since the transform $X \leftarrow \alpha X$ results in the transform $p(x) \rightarrow \alpha^{-1} p(\alpha^{-1}x)$ of the corresponding probability density functions (pdfs), we finally get

$$p(a_{\nu\beta}|N_{\nu\beta}) = \frac{1}{2^{N_{\nu\beta}-1}\Gamma(N_{\nu\beta})\sigma} \left(\frac{2a_{\nu\beta}}{\sigma}\right)^{N_{\nu\beta}-1} e^{-\frac{a_{\nu\beta}}{\sigma}} \tag{17}$$

Then, P_{fa} is given by

$$\begin{aligned} P_{\text{fa}} &= P(\max_{\nu\beta} a_{\nu\beta} > \tau) \\ &= 1 - \prod_{\nu\beta} P(a_{\nu\beta} < \tau) \\ &= 1 - \prod_{\nu\beta} \mathbb{E}_{N_{\nu\beta}} \left[\int_0^\tau p(a_{\nu\beta}|N_{\nu\beta}) da_{\nu\beta} \right] \\ &= 1 - \prod_{\nu\beta} \mathbb{E}_{N_{\nu\beta}} \left[\int_0^\tau \frac{1}{2^{N_{\nu\beta}-1}\Gamma(N_{\nu\beta})\sigma} \Omega e^{-\frac{a}{\sigma}} da \right] \\ &= 1 - \prod_{\nu\beta} P\left(N_{\nu\beta}, \frac{\tau}{\sigma}\right) \end{aligned} \tag{18}$$

where $\Omega = \left(\frac{2a}{\sigma}\right)^{N_{\nu\beta}-1}$ and $P(n, x)$ is the incomplete gamma function:

$$P(n, x) = \int_0^x \frac{1}{\Gamma(n)} t^{n-1} e^{-t} dt. \tag{19}$$

And accounting for the distribution of $N_{\nu\beta}$ we get

$$P_{\text{fa}} = 1 - \prod_{\nu\beta} \left[\sum_{k=0}^{\infty} P\left(k, \frac{\tau}{\sigma}\right) \frac{\left(SN^0_{\nu\beta}\right)^k}{k!} e^{-SN^0_{\nu\beta}} \right]. \tag{20}$$

By plotting P_{fa} as a function τ, one can choose the threshold τ for a given P_{fa}. Note that $P(n, x)$ can be found implemented in many scientific programming libraries, making thus the practical calculation of P_{fa} quite easy. As an example, we have considered a case of a signal without LFMs and three IMFs ($K = 3$) is considered. σ is set to 1. The all-at-one Hough transform and the IMFs are presented on the first line of Fig. 4. On the second line of the figure, we observe the corresponding THH transform output and the false alarm rate as a function of the threshold. The false alarm rate starts decreasing drastically for τ >24, which is in good agreement with the fact that the THH transform output (Fig. 4, bottom left) remains smaller than about 24 ($P_{\text{fa}} = 4.4\%$).

V. DETECTION IN NOISE-FREE ENVIRONMENT

We first test THH transform on free noise signals. For LFM detection, we place a bound 5% on the false alarm probability P_{fa} to determine the threshold τ (20). THH transform is illustrated on two multicomponent signals and detection results are compared with WVD-Hough transform and SPWVD-Hough transform.

A. Results

The first illustration of LFM detection is a signal $x_1(t)$ with four components ($K = 4$) and an observation time

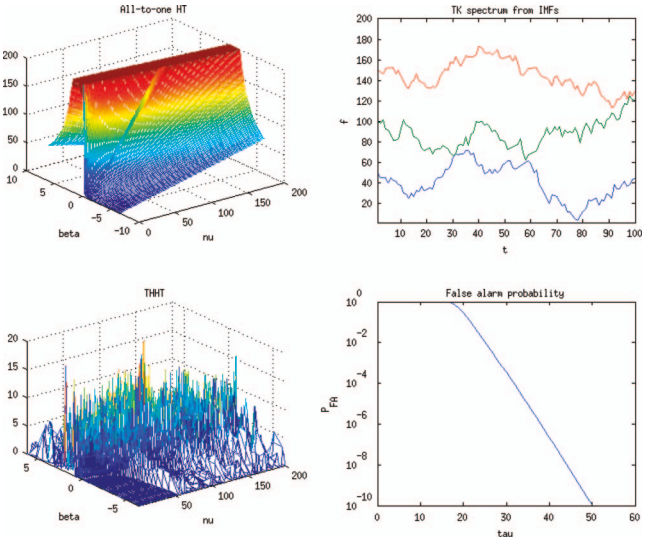

Fig. 4. NP thresholding.

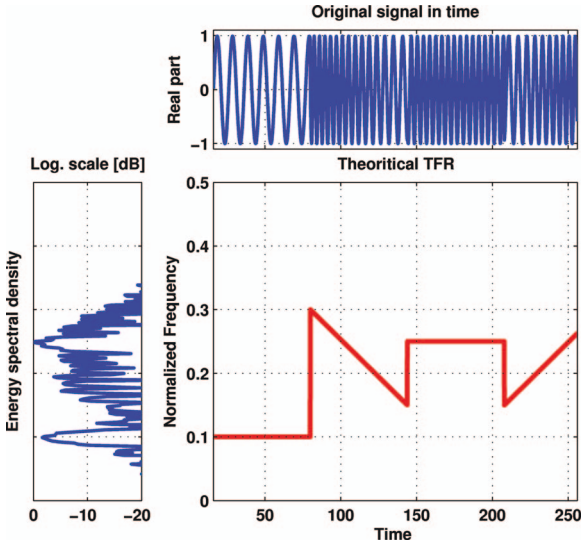

Fig. 5. Ideal time-frequency representation of free noise signal $x_1\ (t)$.

$T = 256$s (Fig. 5). Using (20) with $P_{\text{fa}} = 0.05$, $K = 4$, $T = 256$, and $F_{\text{s}} = 1$Hz we find $\tau = 67$. The associated TH transform, WVD, and SPWVD are shown, respectively, in Figs. 6(a), 8(a), and 10(a). The lines are clearly visible on SPWVD representation and better on TH transform. For WVD, the detection of all IFs is very hard due to the cross-terms (Fig. 8(a)). In Fig. 10(a), the time smoothing carried out by SPWVD considerably reduces these artifacts, but gives the worst resolutions (in time and in frequency). Comparing TH transform against WVD and SPWVD, the four time-frequency components are well localized with no cross-terms or loss in time-frequency resolution (Fig. 6(a)). Hough transform has been applied to these three time-frequency representations. Both THH transform and WVD-Hough transform show four peaks (Figs. 7 and 9). However, the peaks are significantly more prominent in THH transform than in WVD-Hough transform. The estimation of the IFs by THH transform,

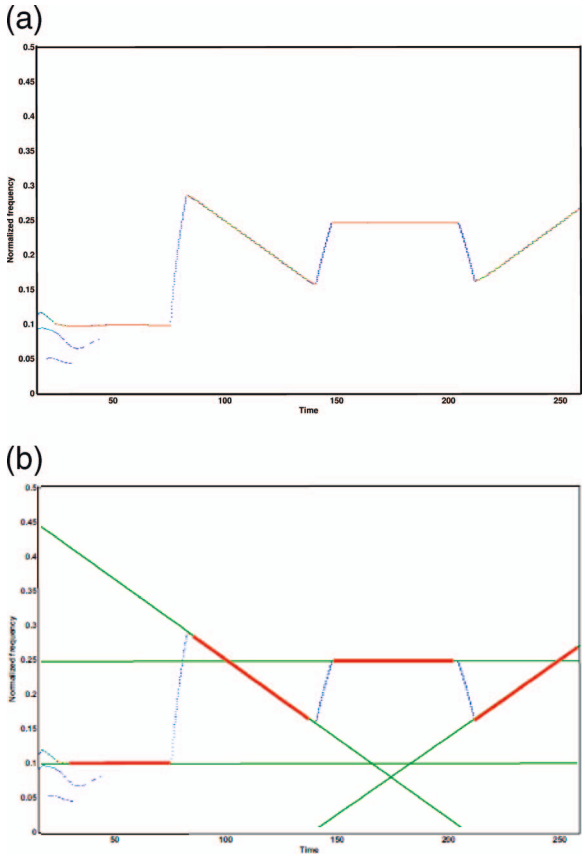

Fig. 6. LFM components tracking in TH transformed plane of $x_1\ (t)$. (a) TH transform of $x_1\ (t)$. (b) Lines of detection on TH transform.

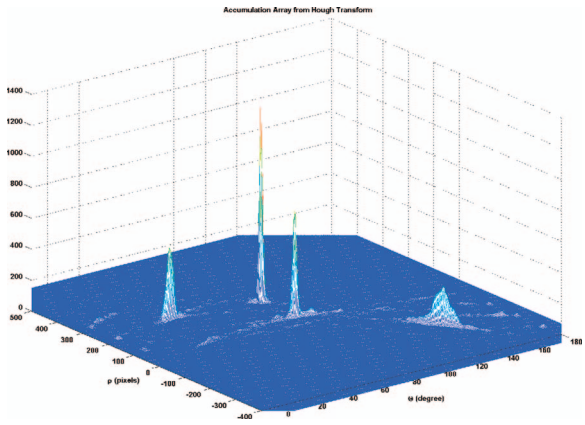

Fig. 7. THH transform applied to $x_1\ (t)$.

WVD-Hough transform, and SPWVD-Hough transform are shown, respectively, in Figs. 6(b), 8(b), and 10(b). Due to oscillating structures of cross-terms, the detection of peak by Hough transform is difficult for the WVD (Fig. 8(b)). While SPWVD reduces the cross-terms and gives a better time-frequency representation, estimation of the IFs remains difficult (Fig. 10(b)). For THH transform, the time-frequency components are well separated in the parameter space (Fig. 7). Unlike WVD-Hough transform, the four time-frequency components are well detected and estimated with the THHT (Fig. 6(b)).

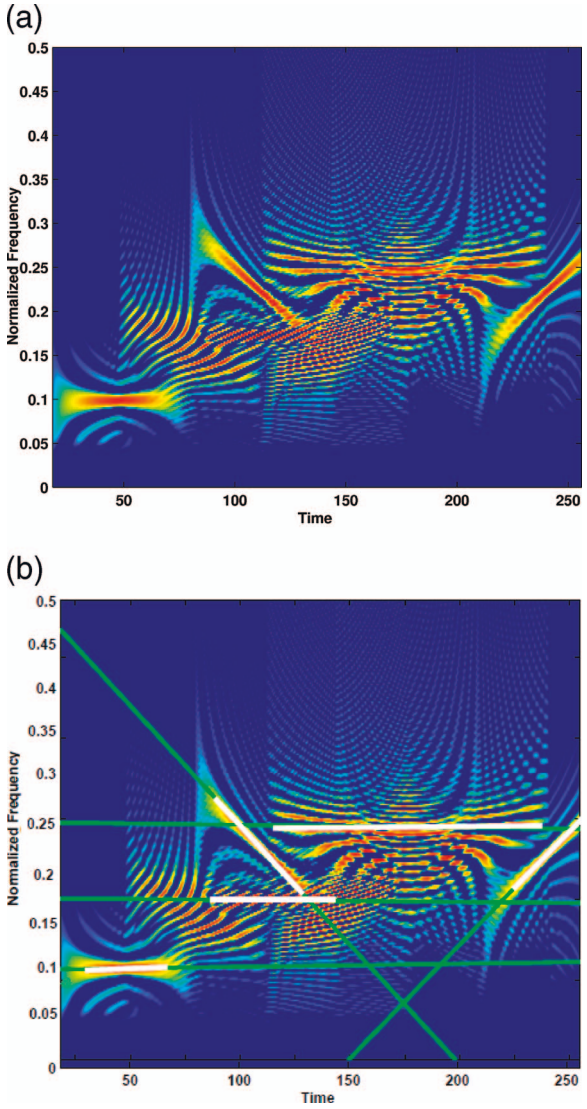

Fig. 8. LFM components tracking in WVD plane for $x_1\ (t)$. (a) WVD of $x_1\ (t)$. (b) LFM detection on WVD.

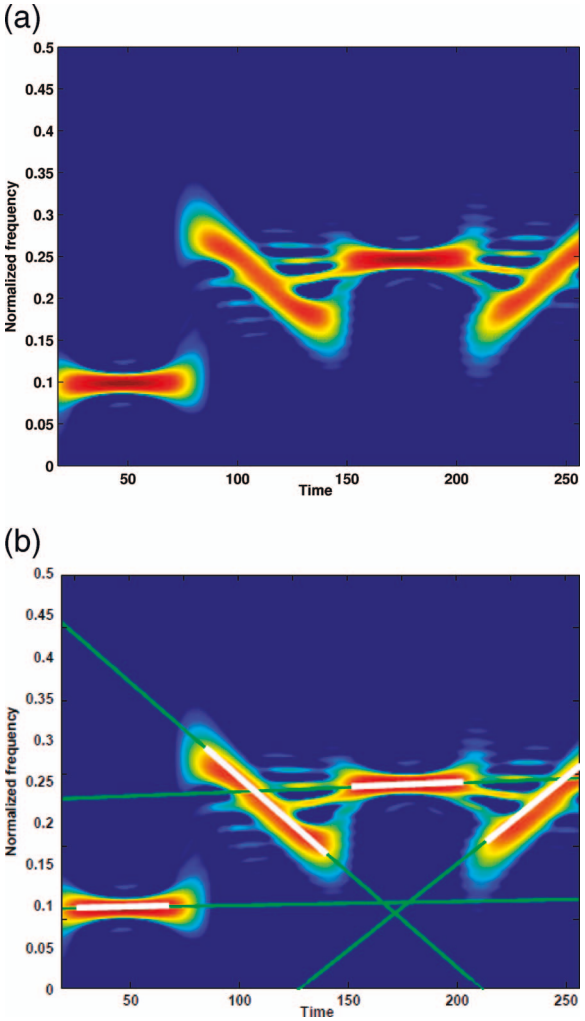

Fig. 10. LFM components tracking in SPWVD plane for $x_1\ (t)$. (a) SPWVD of $x_1\ (t)$. (b) LFM detection on SPWVD.

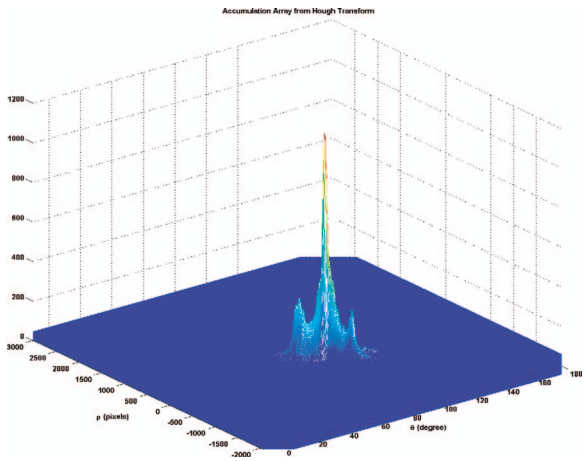

Fig. 9. WVD-Hough transform applied to $x_1\ (t)$.

THH transform has also been tested on a multicomponent signal $x_2(t)$ of seven linear chirps and sinusoidal chirp in the time-frequency domain (Fig. 11). With $K = 8$, we obtain $\tau = 92$. Results of SPWVD and TH transform are shown in Figs. 12 and 13. While the different components are hardly readable in the time representation, they clearly appear in SPWVD and are even better evidenced in TH transform. Again, as in the first case the cross-terms problem is more important as the number of signal components increases and this is well evidenced on the output of SPWVD (Fig. 13(a)). The sinusoidal FM component in SPWVD is represented as an LFM signal (Fig. 13(b)). Note that TH transform is devoid of the cross-terms effect and all IFs are well localized (Fig. 12(a)). However, SPWVD provides cross-terms and so the detection and estimation of IFs are not easy (Fig. 13(b)). Comparing THH transform against SPWVD-Hough transform, all linear IFs components are well detected, localized, and estimated (Fig. 12(b)).

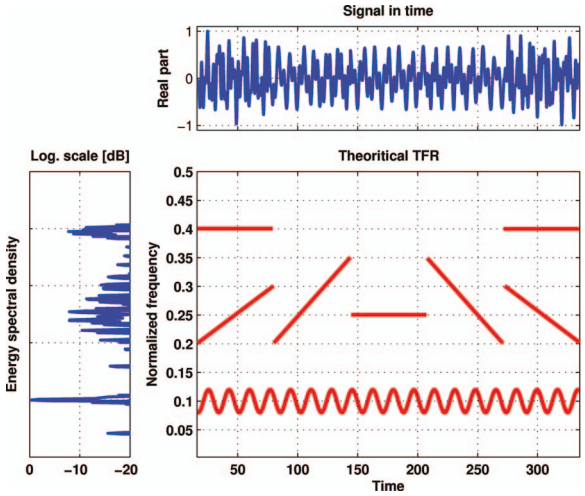

Fig. 11. Ideal time-frequency representation of free noise signal x_2 (t).

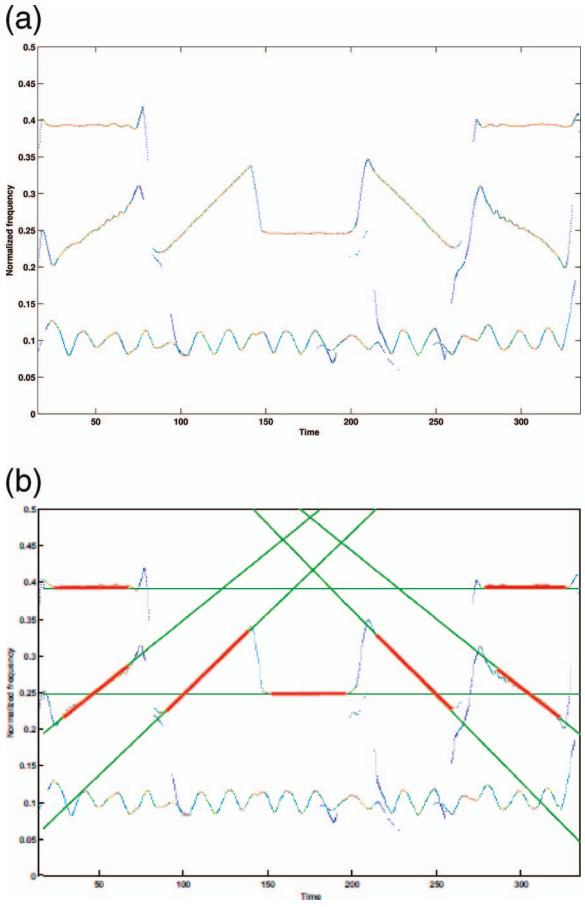

Fig. 12. LFM components tracking in TH transform plane for x_2 (t). (a) TH transform of x_2 (t). (b) Lines of detection on TH transform.

VI. DETECTION IN NOISY ENVIRONMENT

In many applications, signals enhancement or extraction of signals of interest from noise is necessary. Signals or their components may overlap either in time or frequency domain and thus conventional filtering such as time-domain or frequency-domain windowing is not efficient. A solution to this problem is to use subband

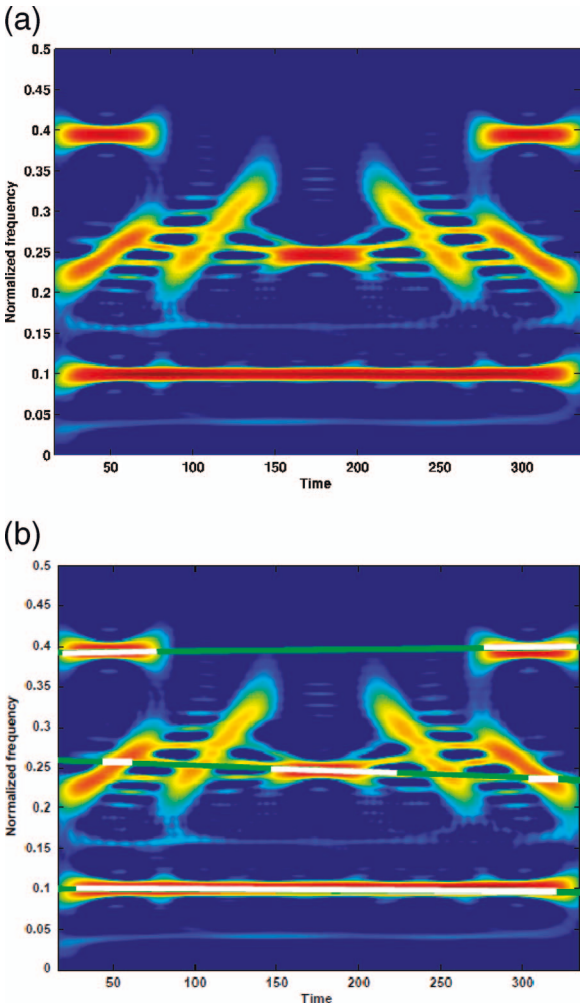

Fig. 13. LFM components tracking in SPWVD plane for x_2 (t). (a) SPWVD of x_2 (t). (b) Lines of detection on SPWVD.

filtering. In this work we use a data-driven time filtering based on EMD where filtering is applied to each extracted IMF.

A. EMD-Based Denoising

A denoised version of an input signal can be obtained by filtering each IMF separately followed by signal reconstruction. Let $f_j(t)$ be a clean deterministic IMF. The j^{th} IMF, corrupted with additive noise $b_j(t)$ is then given by

$$\text{IMG}_j(t) = f_j(t) + b_j(t), where\ j \in \{1, \ldots, K\}. \quad (21)$$

Let $\tilde{f}_j(t)$ be an estimation of $f_j(t)$ based on the noisy observation $\text{IMF}_j(t)$. This estimate is given by

$$\tilde{f}_j(t) = \Gamma[\text{IMF}_j(t), \xi_j] \quad (22)$$

where $\Gamma[., \xi]$ denotes a thresholding or filtering function, with parameters ξ. The denoised signal $\tilde{x}(t)$ is given by [31]

$$\tilde{x}(t) = \sum_{j=1}^{K} \tilde{f}_j(t) + r_K(t). \quad (23)$$

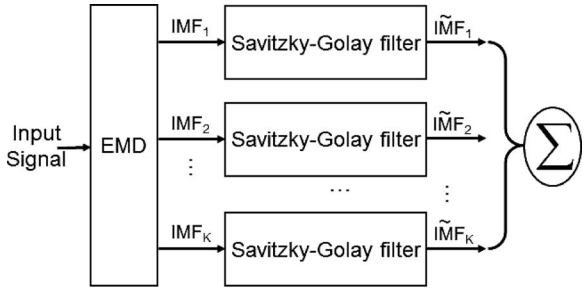

Fig. 14. Block diagram of EMD – SG.

For noise reduction, EMD can be combined with a filtering method such as Savitzky-Golay (SG) smoothing (finite impulse response (FIR) filter) [32] or a nonlinear transformation such as soft-thresholding. If $\Gamma[\mathrm{IMF}_j(t), \xi_j]$ is a filtering method, then ξ_j can be the window size of the filter or its kernel. In this work, we combine EMD with SG filter, which have been shown to be efficient for noise removal [31] (Fig. 14). SG filter (also called digital smoothing polynomial filter) performs time smoothing based on least squares (LS) polynomial fitting across a moving window within the data [32]. This filter performs a local polynomial regression on a distribution of equally spaced points to determine the smoothed value for each data point [32]:

$$\tilde{f}_j(i) = \sum_{m=-M_L}^{m=M_R} \alpha_m.\mathrm{IMF}_j(i+m) \qquad (24)$$

where $i = \ldots, -2, -1, 0, 1, 2, \ldots$. M_L and M_R is the number of points used on the left and right sides of i. The idea of SG filtering is to find filter coefficients α_m (24) that preserve higher moments within the window of analysis. For each point $\mathrm{IMF}_j(i-M_L), \ldots, \mathrm{IMF}_j(i+M_R)$ are determined by using a polynomial of degree p, $\alpha_0 + \alpha_1 i^1 + \alpha_2 i^2 + \ldots + \alpha_p i^p$. The coefficients α_m are given by an LS fit using a shifted windows [32]. SG filter is optimal in the sense that it minimizes the LS error in fitting a polynomial to frames of noisy data. Furthermore, this smoothing filter performs much better than standard averaging FIR filter because it tends to preserve features of the signal such as peak height and high frequency components, which are usually "flattened" by other adjacent averaging techniques.

B. Results

The effectiveness of THH transform has also been tested on noisy LFM signals (13) where the phase function is given by

$$\phi_{\mathrm{LFM}} = 2i\pi\left(\nu t + \frac{\beta}{2}t^2\right). \qquad (25)$$

An LFM signal with $\nu = 0.018$ Hz, $\beta = 0.328$ Hz/s, and $N = 128$ samples is used. White Gaussian noise is added to the LFM signal to obtain noisy signals with signal-to-noise ratios (SNRs) in the range of 50dB down to 5dB. A Monte Carlo simulation with 500 trials is run to evaluate the effectiveness of THH transform estimator. The estimations results of β and ν are presented in 15. For SNR = 5-23dB THH transform provides better β estimates than WVD-Hough transform (Fig. 15). This result was expected due to the cross-terms generated by WVD between free noise signal and noise component. For SNR$\geq$ 23dB the two estimators perform similarly. For ν estimates similar conclusions can be drawn for the estimation (Fig. 15).

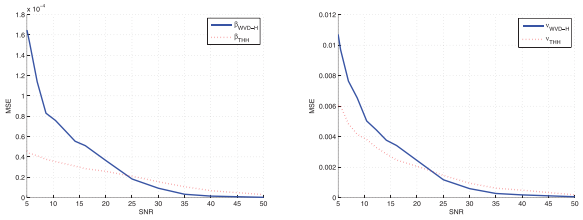

Fig. 15. MSEs of β and ν estimates of noisy LFM signal.

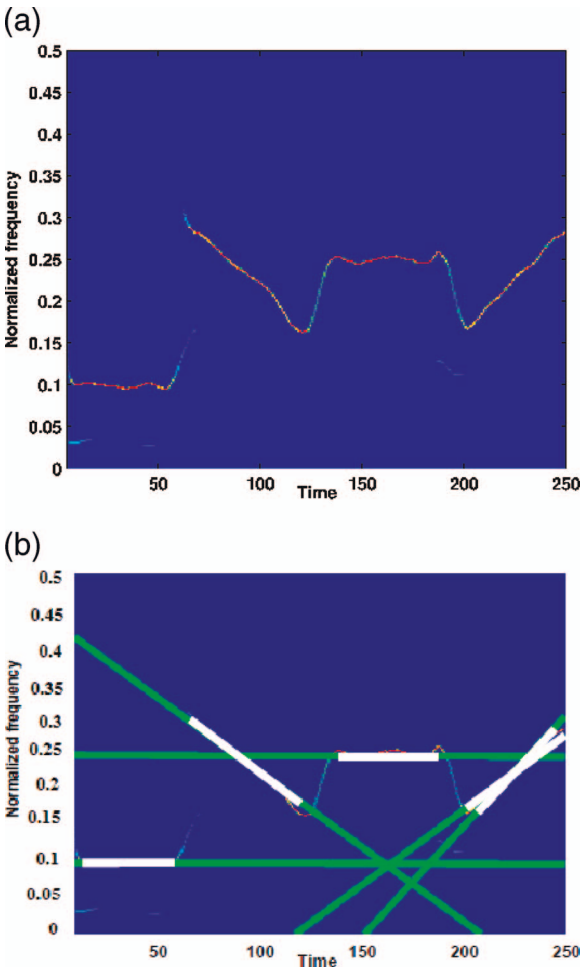

Fig. 16. Components tracking in TH transform plane of x_1 (t). (b) Lines of detection on TH transform.

THH transform is tested on signal $x_1(t)$ (Fig. 5) corrupted with AWGN with an SNR of 7dB. The four IFs are evidenced in both time-frequency representations (Figs. 16(a), 17(a)). The result of line detection with THH and SPWVD-Hough transforms are given in Figs. 16(b)

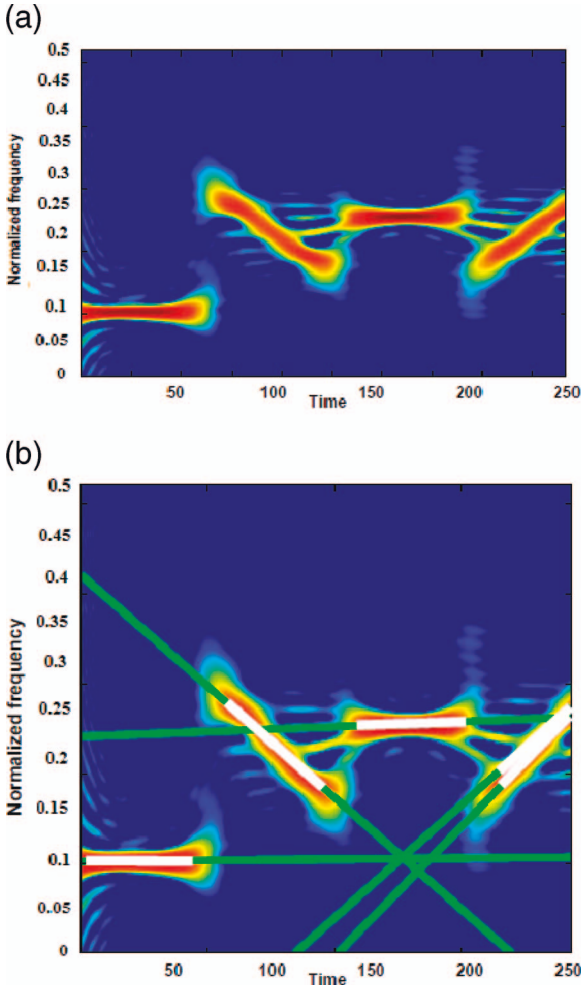

Fig. 17. Components tracking in SPWVD plane of $x_1(t)$ (SNR = 7dB). (a) SPWVD of $x_1(t)$. (b) Lines of detection on SPWVD.

and 17(b), respectively. As in the first simulations, the THH transform (Fig. 16(b)) is sharper than SPWVD-Hough transform (Fig. 17(b)) which makes the detection easier. Both THH and SPWVD-Hough transforms detect correctly three out of four LFM components (Figs. 16(b), 17(b)). The fourth one is not well identified. For THH transform, this may be due to estimation of the IF of the IMF by the TKEO, which has a moderate sensitivity to noise. For the SPWVD-Hough transform, despite the smoothing used, strong cross-terms persist and degrade the time-frequency representation. Consequently both detection and estimation with Hough transform are biased.

Based on EMD and TKEO, TH transform is able to extract the energy associated with different intrinsic time scales of a nonstationary signal such as FM components, and this makes it attractive for detection purpose. Further, TH transform produces a sharp and sparse representation. This is well illustrated on Figs. 6(a), 12(a), and 16(a) where TH transform generates much cleaner, sharper, and sparser time-frequency representations than WVD and SPWVD (Figs. 8(a), 10(a), 13(a), 17(a)). This sparsity and sharpness of TKS are interesting properties for detecting or tracking fine structures such as LFM signals. The detection and localization are also made easy by the TKEO. However, both EMD and TKEO are sensitive to sampling rate. TKEO is best suited for signals with frequency less than one-fourth of the sampling frequency [33]. Thus, in practice, signals must be sampled with sampling rate at least four times the Nyquist-Shannon frequency before applying the ESA. Also, results of the sifting process (IMFs extraction) are influenced by the frequency rate. Based on simulations, it was found that good performances of EMD in terms of IMFs orthogonality and distribution of energy are obtained for a sampling limit of five times Nyquist-Shannon frequency. Thus, prior to applying THH transform the signals must be "sufficiently oversampled."

VII. CONCLUSIONS

In this work a novel approach for detection of multicomponent LFM signals in the time-frequency domain that we called THH transform is proposed. Preliminary results show the interest and effectiveness of THH transform as a tracking method for time-frequency components. THH transform is cross-terms free and does not suffer from the trade-off between time-frequency resolution and cross-terms suppression. No assumptions are made about the number of components of the signal nor their amplitude or phase. Numerical examples show that compared with WVD-Hough and SPWVD-Hough transforms, THH transform achieves better performance in terms of time-frequency components tracking of signals in both noise-free and noisy environments. Furthermore, THH transform yields much sharper results than WVD-Hough and SPWVD-Hough transforms. In all presented examples, LFM components are well identified. In addition, we have developed an NP approach for THH transform detection by estimating the threshold that achieves maximum detection at fixed false alarm rate. Since the performance of THH transform has only been evaluated by some simulations, a large class of signals (extensive simulations) is necessary to confirm the obtained results. As future work we plan to extend the analysis to more complicated IF laws such as nonlinear FM signals or arbitrary time-frequency shapes. Investigation is in progress to optimize the size of the SG filter window to each noisy signal in function, for example, of its SNR.

REFERENCES

[1] Wang, P., Li, H., Djurovic, I., and Himed, B.
Integrated cubic phase function for linear FM signal analysis.
IEEE Transactions on Aerospace and Electronic Systems, **46**, 3 (2010), 963–977.

[2] Peleg, S., and Porat, B.
Linear FM signal parameter estimation from discrete-time observations.
IEEE Transactions on Aerospace and Electronic Systems, **27**, 4 (1991), 607–616.

[3] Guo, J., Zou, H., Yang, X., and Liu, G.
Parameter estimation of multicomponent chirp signals via sparse representation.
IEEE Transactions on Aerospace and Electronic Systems, **47**, 3 (2011), 2261–2268.

[4] Geroleo, F., and Brandt-Pearce, M.
Detection and estimation of LFMCW radar signals.
IEEE Transactions on Aerospace and Electronic Systems, **48**, 1 (2012), 405–418.

[5] Kay, S.
Fundamentals of Statistical Signal Processing: Detection Theory. Upper Saddle River, NJ: Prentice-Hall, 1988.

[6] Bi, G., Li, X., and See, C. S.
LFM signal detection using LPP-Hough transform.
Signal Processing, **91** (2011), 1432–1443.

[7] Abatzoglou, T.
Fast maximum likelihood joint estimation of frequency and frequency rate.
IEEE Transactions on Aerospace and Electronic Systems, **AES-22**, 6 (1986), 708–715.

[8] Djuric, P., and Kay, S.
Parameter estimation of chirp signal.
IEEE Transactions on Aerospace and Electronic Systems, **38**, 12 (1990), 2118–2126.

[9] Lv, X., Xing, M., Zhang, S., and Bao, Z.
Keystone transformation of the Wigner-Ville distribution of multicomponent LFM signals.
Signal Processing, **89**, 5 (2010), 791–806.

[10] Barbarossa, S.
Analysis of multicomponent LFM signals by a combined Wigner-Hough transform.
IEEE Transactions on Signal Processing, **43**, 6 (1995), 1511–1515.

[11] Altes, R.
Detection, estimation and classification with spectrograms.
Journal of the Acoustical Society of America, **67** (1980), 1232–1246.

[12] Wang, M., Chan, A., and Cui, C.
Linear frequency-modulated signal detection using Radon-ambiguity transform.
IEEE Transactions on Signal Processing, **46**, 3 (1998), 571–586.

[13] Hlawatsch, F., and Boudreaux-Bartels, G.
Linear and quadratic time-frequency signal representations.
IEEE Signal Processing Magazine, **9**, 2 (Apr. 1992), 21–67.

[14] Wood, J., and Barry, D.
Linear signal synthesis using the Radon-Wigner transform.
IEEE Transactions on Signal Processing, **42**, 8 (1994), 2105–2111.

[15] Cexus, J.-C., and Boudraa, A.
Nonstationary signals analysis by Teager-Huang transform (THT).
In *EUSIPCO*, Florence, Italy, 2006, pp. 1–5.

[16] Cexus, J.-C., Boudraa, A., and Bouchikhi, A.
A combined Teager-Huang and Hough transform for LFM signals detection.
In *IEEE ISCCSP*, Limassol, Cyprus, 2010, pp. 1–5.

[17] Junsheng, C., Dejie, Y., and Yu, Y.
The application of energy operator demodulation approach based on EMD in machinery fault diagnosis.
Mechanical Systems and Signal Processing, **21** (2007), 668–677.

[18] Li, H., Zhang, Y., and Zheng, H.
Bearing fault detection and diagnosis based on order tracking and Teager-Huang transform.
Journal of Mechanical Science and Technology, **21** (2007), 811–822.

[19] Li, H., Zheng, H., and Tang, L.
Gear fault detection based on Teager-Huang transform.
International Journal of Rotating Machinery, **2010** (2010), 1–9.

[20] Benramdane, S., Cexus, J.-C., Boudraa, A., and Astolfi, J.
Time-frequency analysis of pressure fluctuations on a hydrofoil undergoing a transient pitching motion using Hilbert-Huang and Teager-Huang transforms.
In *Pressure Vessels and Piping Conference*, San Antonio, TX, 2007, pp. 199–207.

[21] Kaleem, M., Sugavaneswaram, L., Guergachi, A., and Krishnan, S.
Application of empirical mode decomposition and Teager energy operator to EEG signals for mental task classification.
In *Proceedings of IEEE EMBS*, 2010, pp. 4590–4593.

[22] Barkoula, K., Ifantis, A., and Economou, G.
Long term geo-electric potential signal analysis using the Teager Huang transform.
In *8th IASTED International Conference on Signal Processing, Pattern Recognition, and Applications*, Innsbruck, Austria, 2011, pp. 245–252.

[23] Huang, N., Shen, Z., Long, S., Wu, M., Shih, H., Zheng, Q., Yen, N., Tung, C., and Liu, H.
The empirical mode decomposition and Hilbert spectrum for nonlinear and nonstationary time series analysis.
Proceedings of the Royal Society A, **454** (1998), 903–995.

[24] Maragos, P., Kaiser, J., and Quatieri, T.
On separating amplitude from frequency modulations using energy operators.
In *ICASSP*, San Francisco, CA, Mar. 1992, pp. 1–4.

[25] Cohen, L.
Time-Frequency Analysis, Englewood Cliffs, NJ: Prentice-Hall, 1995.

[26] Duda, R., and Hart, P.
Use of the Hough transformation to detect lines and curves in pictures.
Communications of the ACM, **15**, 1 (1972), 11–15.

[27] Cirillo, L., Zoubir, A., and Amin, M.
Parameter estimation for locally linear FM signals using a time-frequency Hough transform.
IEEE Transactions on Signal Processing, **56**, 9 (2008), 4162–4175.

[28] Barbarossa, S., and Lemoine, O.
Analysis of nonlinear FM signals by pattern recognition of their time-frequency representation.
IEEE Signal Procesing. Letters, **3**, 4 (1996), 112–115.

[29] Kay, S., and Boudreaux-Bartles, G.
On the optimality of the Wigner distribution for detection.
In *ICASSP*, Mar. 1985, pp. 1017–1020.

[30] Barbarossa, S., and Scaglione, A.
Adaptive time-varying cancellation of wideband interference in spread spectrum communications based on time-frequency distributions.
IEEE Transactions on Signal Processing, **47**, 4 (1999), 957–965.

[31] Boudraa, A., and Cexus, J.-C.
Denoising via empirical mode decomposition.
In *IEEE ISCCSP*, Marrakech, Morocco, Mar. 2006, pp. 1–4.

[32] Savitzky, A., and Golay, M.
Smoothing and differentiation of data by simplified least squares procedures.
Analytical Chemistry, **36** (1964), 1627–1639.

[33] Kaiser, J.
On a simple algorithm to calculate the energy of a signal.
In *Proceedings of ICASSP*, Albuquerque, NM, 1990, pp. 381–384.

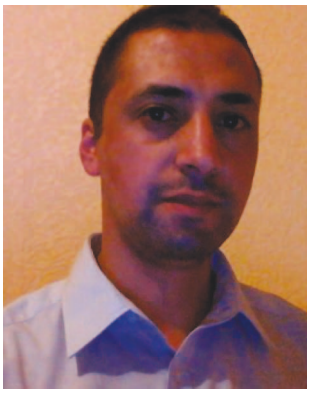

Abdelkhalek Bouchikhi was born in Frenda, Algeria, in 1979. He received the engineer degree in Telecoms Systems from the Institute of Telecommunications, Oran, Algeria, in 2002. After an industrial experience within the ZTE corporation, in 2003, he prepared the DEA of Acoustics at University of Marseille, in 2004. Then, he received the Master degree in signal and image processing and Ph.D. degree in signal processing from the University of Rennes 1, France in 2005 and 2010, respectively. From 2006 to 2010, he joined Ecole Navale, Brest, France, as an Research and Teaching Assistant. From 2010 to 2012, he joined the Ecole Nationale d'Ingénieurs de Brest as an Assistant Professor. He is currently PostDoc with ROSA team of ICD-UTT. His current research interests include signal and image processing, acoustics, Radar and Sonar targets detection and identification, and electrical machines anomalies detection and identification.

Abdel-Ouahab Boudraa was born in Constantine, Algeria. He received the B.S. degree in Physics (Electronics Engineering) from Constantine Institute of Physics, University of Constantine, Algeria, and the Engineer degree in Electronics from Educatel (Liege, Belgium). He also received the M.S. degree in Biomedical Engineering from INSA, Lyon, University degree in Nuclear Magnetic Resonance, the Ph.D. degree in Image Processing and the University degrees in Statistics and Modeling and in Positron Emission Tomography all from the University of Lyon 1, France. He is currently Associate Professor of Electrical Engineering at Ecole Navale, Brest, France. His current research interests include computer vision, vector quantization, data structures and analysis, data fusion, time frequency analysis, higher-order energy operators, empirical mode decomposition, hard and fuzzy pattern recognition.
Dr. Boudraa is recipient of 2003 Varian Prize awarded by the Swiss Society of Radiobiology and Medical Physics for the best published paper impacting Radiation Oncology. Dr. Boudraa is a Senior Member IEEE.

Jean-Christophe Cexus received his engineering degree and MSc degree in control from l′Ecole Supérieure des Sciences Appliquées pour l′Ingénieur de Mulhouse (ESSAIM) and PhD degree in Signal processing from University of Rennes 1. He is currently Assistant professor at ENSTA Bretagne. His research interests include time-frequency analysis, empirical mode decomposition, Radar, Sonar target recognition, and neural networks.

Thierry Chonavel received the Ph.D. degree from Télécom ParisTech, Paris, France, in 1992. Since 1995, he has been with the Institut Télécom, Télécom Bretagne, Brest, and CNRS LabSTICC (UMR 6285) where he is a Professor. He has been involved in signal processing research activities ranging from array processing, underwater acoustic transmission, and seismic signals deconvolution to spread-spectrum communications. He has also worked on projects related to GPS-Galileo receivers, radar processing, and waveform design for Radars and Sonars, MIMO techniques for powerline communications and speech synthesis and compression.